Engineering Science and Technology, an International Journal xxx (xxxx) xxx

HOSTED BY

Contents lists available at ScienceDirect

Engineering Science and Technology, an International Journal

journal homepage: www.elsevier.com/locate/jestch

Full Length Article

AGC performance amelioration in multi-area interconnected thermal and thermal-hydro-gas power systems using a novel controller

Yogendra Arya [a,*], Pankaj Dahiya [b], Emre Çelik [c], Gulshan Sharma [d], Haluk Gözde [e], Ibraheem Nasiruddin [f]

[a] Department of Electrical & Electronics Engineering, Maharaja Surajmal Institute of Technology, Janakpuri, New Delhi, India
[b] Department of Electronics & Communication Engineering, Delhi Technological University, Shahbad Daulatpur Village, Rohini, Delhi, India
[c] Department of Electrical & Electronics Engineering, Engineering Faculty, Duzce University, Düzce, Turkey
[d] Department of Electrical Power Engineering, Durban University of Technology, Durban 4001, South Africa
[e] Department of Electronics and Communication Engineering, National Defence University, Turkish Military Academy, Ankara, Turkey
[f] Department of Electrical Engineering, Jamia Millia Islamia, Jamia Nagar, Okhla, New Delhi, Delhi, India

ARTICLE INFO

Article history:
Received 24 April 2020
Revised 12 August 2020
Accepted 29 August 2020
Available online xxxx

Keywords:
Multi-source thermal-hydro-gas power system
Reheat thermal power system
Optimal fractional order fuzzy controller
Interconnected electric power system
Generation control of energy system
Robust control operation

ABSTRACT

Due to varying structure, random load demands, nonlinearities, parameters ambiguity, steadily escalating size and intricacy of the interconnected power system (IPS), automatic generation control (AGC) is treated as one of the biggest crucial issues in IPS. Hence, expert, intelligent and robust control scheme is indispensable for stable operation of IPS and supply of electricity under sudden load demand disturbances. In vision of this, in this work, a novel cascade fuzzy-proportional integral derivative incorporating filter (PIDN)-fractional order PIDN (FPIDN-FOPIDN) controller is offered as an expert control strategy to deal effectively with AGC issue of IPS. Imperialist competitive algorithm is prolifically utilized for optimizing the controller parameters. Initially, a two area non-reheat thermal IPS is studied in detail and next to attest the efficacy of the technique, the study is extended to realistic two-area multi-source thermal-hydro-gas and reheat thermal three-area systems. The prominent benefit of cascade FPIDN-FOPIDN strategy comprises its great lethargy to large load demands and its supremacy over various latest intelligent classical/fuzzy controllers. The control strategy beats several techniques concerning significant lesser settling time, oscillations, over/under shoots and different performance index values. Finally, a robustness investigation is performed in order to validate the robustness of the controller.

1. Introduction

The power system (PS) is a complex and huge system containing various control areas unified together through the tie-lines to transfer power among them. The intricacy of the modern interconnected PS (IPS) has amplified many folds due to rising energy necessities day by day with the growing population. Additionally, the load demand on IPS is continuously fluctuating and the variation in load demand at one-area will cause the transient aberration in frequency, generation and tie-line flow throughout the PS. The mismatch between the generation and demanded power is the main cause of these deviations. Hence, currently, the control and operation of IPS have become very problematic and challenging. AGC is the strategy via which equilibrium between the power generation and power demand is attained thus it preserves the tie-line flows and PS frequency within recommended edges [1]. It enables the synchronous generators of control areas to regulate their generations in view of the load demands achieving zero steady state errors to maintain the synchronism of PS regardless the changes in load demands. Inappropriate design of AGC system may worsen the system performance initiating large oscillations in generation, system frequency and power flows of tie-line which may force the system towards instability. Thus, AGC necessitates the use of a suitable control strategy for effective control/operation of modern IPS as critically and comprehensively reviewed in [2,3].

Various optimization and control techniques such as whale optimization algorithm (WOA) based two-degree-of-freedom state feedback controller (2-DOF-SFC) [1], distributed model predictive control (MPC) [4–6], optimal [7,8], optimal output feedback [9], hybrid stochastic fractal search-pattern search (hSFS-PS) tuned cascade PI-PD [10], differential evolution algorithm (DEA) optimized PID [11], teaching learning based optimization (TLBO) optimized PID [12], imperialist competitive algorithm (ICA) optimized PID [13], jaya algorithm (JA) optimized PID-filter (PIDN) [14],

* Corresponding author.
E-mail address: mr.y.arya@gmail.com (Y. Arya).
Peer review under responsibility of Karabuk University.

https://doi.org/10.1016/j.jestch.2020.08.015

symbiotic organisms search (SOS) algorithm based PID/PIDN [15,16], hybrid invasive weed optimization-PS (hIWO-PS) optimized 2-DOF-PID [17], sine cosine algorithm (SCA) tuned cascade FOPI-FOPID [18] and WOA optimized cascade IDN-FOPD [19] controllers are conveyed in the up-to-date literature for effective AGC of diverse kinds of traditional and restructured IPS. The classical controllers stated above optimized for a definite working situation, sometime might not work efficiently specifically in IPS where operating condition changes with continuously varying load demands. Hence, to improve AGC performance fuzzy logic controller (FLC) is suggested in place of classical controller.

Various studies have been conducted to propose various structures of FLC optimized by different soft computing techniques in [20–30]. Recently, hybrid particle swarm optimization-PS (hPSO-PS) [20]/ICA [21] techniques are utilized to tune scaling factors (SFs) of output and/or input of fuzzy PI (FPI) controller. To advance the recital of FPI, some researchers for different types of power systems (PSs) have suggested various optimization methods to tune input/output SFs of FPID controller such as hybrid PSO-levy flight algorithm (hPSO-LFA) [22], hybrid local unimodal sampling-TLBO (hLUS-TLBO) [23–24], hybrid harmony search-cuckoo optimization algorithm (hHS-COA) [25], mine blast algorithm (MBA) [26], hybrid improved firefly algorithm-PS (hIFA-PS) [27] and hybrid differential evolution-PSO (hDE-PSO) [28]. A fuzzy gain scheduled PID (FGS-PID) controller is proposed in [29] for a hybrid photovoltaic-battery system. An ICA tuned FPIDN double-I controller is projected in [30]. In FPID controller, as its derivative is distressed by upper frequency noise signal, a first order filter is engaged in derivative block to diminish upper frequency noise to acquire FPID with filter (FPIDN) controller. In the literature, few researchers have proposed FPIDN controller with input/output SFs decided consuming hLUS-TLBO [24] and ICA [30] techniques. Amalgamation of fuzzy with artificial neural networks are also emerging to attain better results as demonstrated in [31–33].

Recently, the practices of the fractional order (FO) controllers are acting more in the literature since they offer extra flexibility and robustness in the control processes [18,19,34–37]. Big bang big crunch algorithm (BBBCA) [34] and ICA [35] based FOPID outperforms conventional PID controller for regulated and deregulated PSs. Next, cascaded FO controllers like SCA based FOPI-FOPID [18], WOA based IDN-FOPD [19] and volleyball premier league algorithm (VPLA) based 2DOF-PI-FOPDN [36] perform superiorly in different PS structures. Recently, the literature review indicates the application of the hybridized FLC-FO controllers in PS such as ICA based FPIDN-FOI [37]/FFOID [38]/FFOPI-FOPD [39] and ant lion optimiser (ALO) [40]/biogeography-based optimization [41]/ICA [42] based FO fuzzy PID (FOFPID) controllers. These controllers display better results in comparison to FLC and FO controllers for various multi-area traditional/restructured PSs. However, the performance assessment of cascade fuzzy PIDN-FOPIDN (FPIDN-FOPIDN) structured controllers has bot been discovered so far. Considering these facts, a cascade FPIDN-FOPIDN control strategy is offered for multi-area AGC IPS models.

In realistic PSs, each control area incorporates dissimilar generation sources like hydro, thermal, gas, etc. [1,7–12,16,18–21,23–25,27,30,37–39,41–42]. As such there is an indispensable requirement of extensive research on multi-source AGC systems. Therefore, in the current work, the authors have also pondered a pragmatic two-area IPS having diverse power sources comprising thermal, hydro and gas power plants in each area. Some other existing multi-source systems are wind-combined heat and power (CHP) [43] and photovoltaic-wind turbine-micro turbine-energy storage scheme [44–45].

In addition to the structure of the controller employed, the recital of the system also hinges predominantly on apposite selection of tuning practice exploited for optimizing the parameters of the controller. Moreover, it is perceived that so far insufficient works have been executed with FPIDN structured AGC control strategy [24,30]. However, in the literature, the application of cascade FPIDN-FOPIDN controllers in single/multi-source AGC system is unattainable. Therefore, the study of FPIDN/cascade FPIDN-FOPIDN controller in multi-area AGC of single-source thermal as well as multi-source thermal-hydro-gas systems is required. Due to better convergence rate, scarcity in AGC applications, robust search performance of ICA against nonlinearities, constraints and parameters uncertainties, the optimal fine-tuning of PIDN/FPIDN

Description of symbols

P_r	rated area capacity	a,c	constants of valve positioner
α_{12}	area size ratio	b	TC of valve positioner
F^0	nominal frequency of PS	T_{CR}	GT combustion reaction time delay
R	speed governor (SG) regulation parameter	T_F	GT fuel TC
B	frequency bias constant	T_{CD}	GT compressor discharge volume TC
β	frequency response characteristics	K_T	thermal power generation contribution
K_{PS}	PS gain	K_H	hydro power generation contribution
T_{PS}	PS time constant	K_G	gas power generation contribution
T_G	SG time constant (TC)	ΔP_g	incremental deviation in area generation
T_T	thermal turbine TC	ΔP_D	incremental deviation in load demand in area
K_r	reheater gain	ΔP_G	incremental deviation in generating unit output
T_r	reheater TC	J	Cost function
T_{12}	tie-line synchronizing coefficient	FO	fractional order
T_{RH}	hydro turbine (HT) SG transient droop TC	IPS	Interconnected power system
T_R	HT SG reset time	AGC	Automatic generation control
T_{GH}	HT SG main servo TC	ICA	imperialist competitive algorithm
T_W	nominal starting time of water in penstock	TANRT	two-area non-reheat thermal
X	gas turbine (GT) SG lead TC	TART	three-area reheat thermal
Y	GT SG lag TC	MSTATHG	multi-source two-area thermal-hydro-gas

and the cascade FPIDN-FOPIDN controller parameters is attained using ICA.

1.1. Problem challenges

The fluctuations in load demand causes the discrepancies between the generation and demand resulting into variation in system frequency and tie flows from their corresponding supposed values. The main challenges to resolve this problem are

(i) To effectively alleviate the variations in system frequency, generation and tie-line flows from their stated borders via utilizing a new AGC controller.
(ii) The selection of an appropriate optimization technique to adjust the factors of the designed controller.
(iii) The designed controller should deliver system responses having least settling time, under shoots and over shoots.
(iv) The designed control technique should outperform the existing control strategies.
(v) The designed technique should provide superior performance if implemented on different PS models.
(vi) The designed technique should be robust in nature.

1.2. Main objectives and contributions

The main objectives and the innovative contributions of this work are itemized as follows:

(i) To recommend a novel ICA tuned cascade FPIDN-FOPIDN configured controller for AGC problem solution of interconnected two-area non-reheat thermal PS.
(ii) To determine the advantages of the projected control strategy in comparison to ICA/JA optimized PIDN, hPSO-PS/PSO/PS optimized FPI, hIFA-PS/hHS-COA tuned FPID and ICA/hLUS-TLBO tuned FPIDN controllers.
(iii) To outspread the work to the existing realistic diverse-source two-area thermal-hydro-gas PS.
(iv) To validate the superiority of the method compared to the existing intelligent control strategies like optimal output feedback, DE/hSFS-PS/TLBO based PID, DE based FPID and ICA based FPIDN/FOFPID controllers developed for the above stated system.
(v) To extend the study to a single-source three-area reheat thermal PS.
(vi) To demonstrate the value of the suggested controller over SOS optimized PID, SOS/ICA optimized PIDN, hDE-PSO/hPSO-LFA optimized FPID, ICA optimized FPIDN and hIWO-PS optimized 2DOF-PIDN controllers designed for the PS stated in (v).
(vii) To explore the robustness of advocated controller under consideration of ±20% disparities in the parameters of the systems, variable demand requirements and GRC.
(viii) To scrutinize the consequence of different GRC values on the system performance.

Hence, the main innovation of the presented work is to design a novel optimal cascade FPIDN-FOPIDN controller which offers an enhanced dynamic performance in comparison to other already published works for different PS models. The rest of this study is organized as follows: Section 2 provides a description of examined PS models, Section 3 introduces details of the controller design, Section 4 gives deep analysis of the results, Section 5 presents robustness study and Section 6 offers final conclusion of the study.

2. Studied PS models

The studied PSs are interconnected two-area non-reheat thermal (TANRT) PS displayed in Fig. 4 [14,20,25,27], realistic multi-source two-area thermal-hydro-gas (MSTATHG) PS displayed in Fig. 6 [9,42] and unequal three-area reheat thermal (TART) PS displayed in Fig. 8 [15,28]. The TANRT system has one non-reheat type of turbine and TART system involves of one single reheat type of turbine in individual area. The MSTATHG system consists of one reheat thermal, one hydro (mechanical governor) and one gas generating units in each control area. Ratings of each area of TANRT and MSTATHG systems is 2000 MW. TART system has ratings of area-1, area-2 and area-3 as 2000 MW, 5000 MW and 8000 MW, in order. The exhaustive modelling of the PSs is offered in the references given above. A biasing B = β is contemplated in each area. The data utilized in simulations is given in Appendix. MATLAB/SIMULINK R2015b is employed for codings, models and results of the systems. The description of symbols is provided in Section 1.

3. Controller design

3.1. Controller assembly

The traditional PID controller with fuzzy logic has demonstrated better flexibility and performance to meet the challenges in PS control. In the literature on AGC, majorly controllers like FOPID/PIDN/PID/PI with FL are recommended [20–30,37–42]. But, cascade fractional order (FO) fuzzy logic controller (FLC) has not been observed so far. Therefore, in the present work, a cascade FPIDN-FOPIDN AGC controller is suggested for multi-area PSs as a proficient, intelligent and vigorous controller. The organization and design of the controller is revealed in Fig. 1(a). The controller configuration consists of a FLC, PID with filter (PIDN) and FOPIDN controllers connected in cascade. The FLC has two inputs signals, i.e., ACE and its derivative. Area-1 ACE (ACE_1), area-2 ACE (ACE_2) and area-3 (ACE_3) in two and three-area PSs is specified by Eqs. (1)-(2).

$$\left.\begin{aligned} ACE_1 &= \beta_1 \Delta F_1 + \Delta Ptie_{12} \\ ACE_2 &= \beta_2 \Delta F_2 + \alpha_{12} \Delta Ptie_{12} \end{aligned}\right\} (Two-area\ system) \quad (1)$$

$$\left.\begin{aligned} ACE_1 &= \beta_1 \Delta F_1 + \Delta Ptie_1 \\ ACE_2 &= \beta_2 \Delta F_2 + \Delta Ptie_2 \\ ACE_3 &= \beta_3 \Delta F_3 + \Delta Ptie_3 \end{aligned}\right\} (Three-area\ system) \quad (2)$$

where, frequency response characteristic is represented by β, change in frequency by ΔF, change in tie-line flow by $\Delta Ptie_{ij}/\Delta Ptie_i$, area rating ratio by α_{ij}. Here, $\Delta Ptie_1 = \Delta Ptie_{12} + \Delta Ptie_{13}$, $\Delta Ptie_2 = \alpha_{12}\Delta Ptie_{12} + \Delta Ptie_{23}$ and $\Delta Ptie_3 = \alpha_{13}\Delta Ptie_{13} + \alpha_{23}\Delta Ptie_{23}$.

The FLC output y is the PIDN input and FPIDN-FOPIDN output is the control input ΔP_C for PS (3).

$$\Delta Pc = \left[\left\{\left(yK_P + \frac{yK_I}{s} + \frac{yK_D sN}{s+N}\right) - \Delta F\right\} \times \left(K_{P1} + \frac{K_{I1}}{s^{\lambda}} + \frac{K_{D1} s^{\mu} N1}{s^{\mu} + N1}\right)\right] \quad (3)$$

The FOPIDN controller is the extension of the conventional integer order PIDN controller with their gains having fractional integral–differential orders. The transfer function depiction of PIDN and FOPIDN controllers is stated via Eqs. (4)–(5).

$$C(s) = K_P + \frac{K_I}{s} + \frac{K_D sN}{s+N} (PIDN) \quad (4)$$

$$C(s) = K_{P1} + \frac{K_{I1}}{s^{\lambda}} + \frac{K_{D1} s^{\mu} N1}{s^{\mu} + N1} (FOPIDN) \quad (5)$$

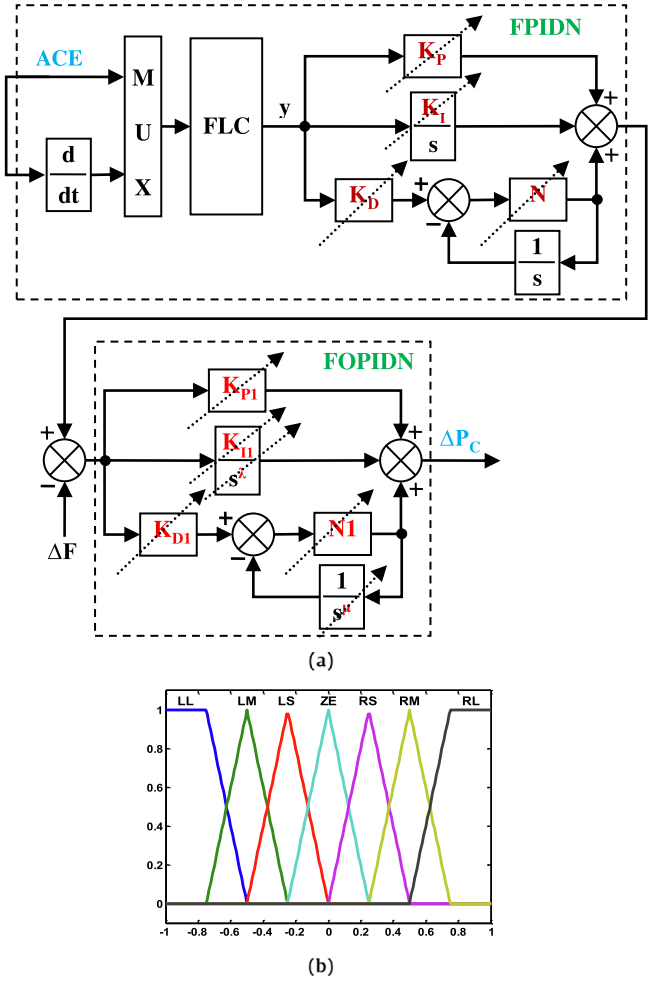

Fig. 1. The controller: (a) structure of cascade FPIDN-FOPIDN controller and (b) controller MFs [25].

In (3)–(5), N/N1 is the filter coefficient. From numerous approximations such as Matsuda, Carlson, low-frequency continued fraction approximation, high-frequency continued fraction approximation, the CRONE approximation submitted by Oustaloup is employed to instrument the integro-differential operators in frequency domain [18]. CRONE employs a recursive scattering of A poles and A zeros forming a TF (transfer function) inside the prestated frequency limits [ω_L, ω_H] [18]. In this work, ω_L = 0.01 rad/s, ω_H = 100 rad/s and A = 6 are taken [21]. More descriptions about FO controllers are available in [18–19,34–42].

To develop cascade FPIDN-FOPIDN, its gains i.e., K_P, K_I, K_D, N, K_{P1}, K_{II}, λ, K_{D1}, μ and N1 are to be selected. For FPIDN controller, seven MFs are engaged for inputs/output. The five internal MFs have triangular shapes and the outer two trapezoidal as showcased in Fig. 1(b) [21]. The designed rules are tabled in Table 1 [21]. The fuzzy linguistic variables LL, LM, LS, ZE, RS, RM and RL represent Left Large, Left Medium, Left Small, Zero, Right Small, Right Medium and Right Large, respectively. To alleviate optimization complexity, input scaling factors of FLC are left at unity and only output scaling factors are tuned. The crisp output of FLC is decided by utilizing center of gravity defuzzification criterion. Furthermore, the Mamdani fuzzy inference engine is also employed.

Governing of two consecutive processes gives the idea of cascade control (CC). CC comprises of multi-control loops and can enhance the control system results compared to single-control loop. It works impressively in rejecting disturbances hastily to give improved system results [18]. The basic CC system includes two control loops as shown in Fig. 2. In Fig. 2, primary/master/outer controller $C_1(s)$ is FPIDN and secondary/slave/inner controller $C_2(s)$ is FOPIDN. The outer control process is $G_1(s)$ and the entire control process is exposed to $d_1(s)$ load disturbance creating Y(s) output. The outside control process input is $U_1(s)$ which is the output of the inner process. The output of outer control process necessarily be controlled to achieve R(s) reference signal. The internal control loop performs as slave. It mitigates the influences of internal process disruptions on the outer control loop. The internal control loop comprises the inner process $G_2(s)$ and $U_2(s)$ the inner process input.

3.2. ICA

Imperialist competitive algorithm (ICA), inspired from sociopolitical strategy is a *meta*-heuristic and stochastic search technique which was introduced by Atashpaz and Lucas [46]. Similar to various evolutionary optimization methods, ICA starts with an initial set of solutions named population. Every fellow of population is an array labelled as country. Each country is parted in two parts; imperialist states and colonies. Few countries with fewer costs are treated as the imperialist states, however, rest countries are treated as their colonies. The imperialist states and their colonies constitute the empires. Allocating the colonies to every empire is dependent on the power or cost of each imperialist state.

This power is inversely proportional to the cost of empires. An empire with more power attracts more colonies. The chief core

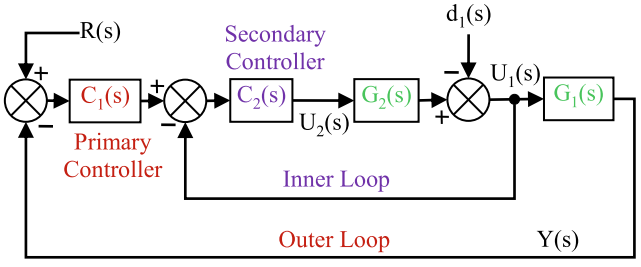

Fig. 2. Cascade controller model.

Table 1
Rule base employed in the controller.

ACE	ACE derivative						
	LR	LM	LS	ZE	RS	RM	RL
LL	RL	RL	RL	RM	RM	RS	ZE
LM	RL	RM	RM	RM	RS	ZE	LS
LS	RL	RM	RS	RS	ZE	S	LM
ZE	RM	RM	RS	ZE	LS	LM	LM
RS	RM	RS	ZE	LS	LS	LM	LL
RM	RS	ZE	LS	LM	LM	LM	LL
RL	ZE	LS	LM	LM	LL	LL	LL

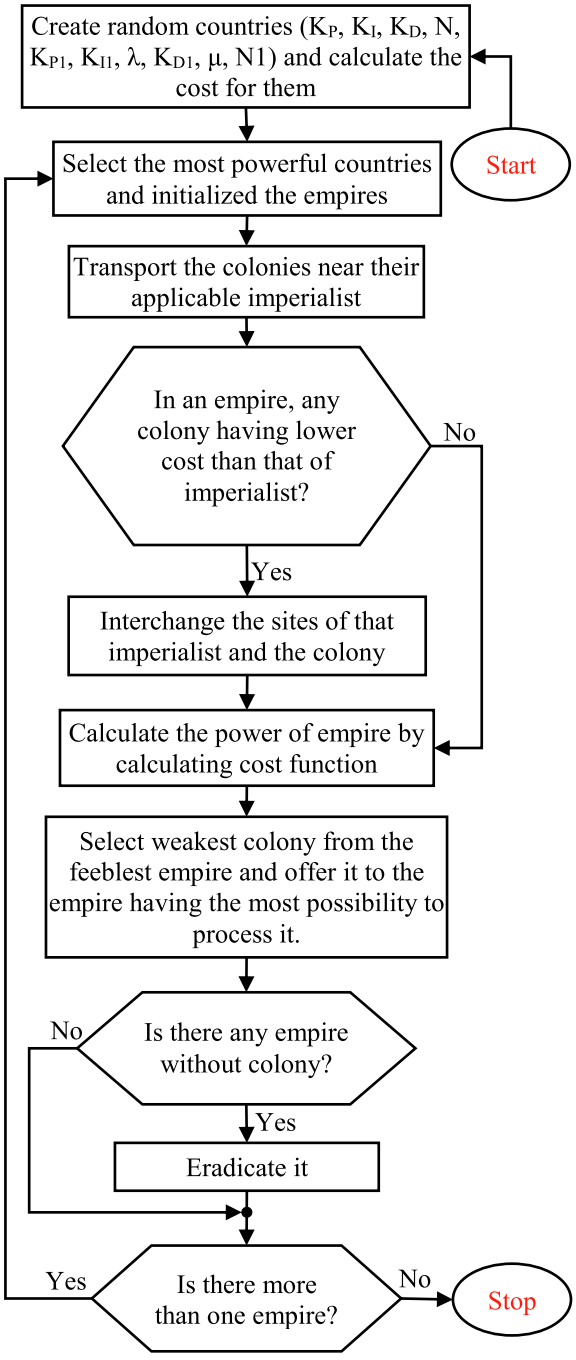

Fig. 3. ICA flow chart.

of ICA is comprised of the imperialistic competition among the empires.

During the iterations of ICA, empires compete to retain more colonies. Empires with more power have higher likelihood to own more colonies and empires with less power will progressively drop their colonies. When all the colonies are controlled by a single imperialist, the algorithm terminates. The main steps concerned to decide the optimal parameters of the controller via ICA are (i) load the empires (ii) travel the colonies towards their pertinent imperialist (Assimilation) (iii) replacing positions of a colony and the imperialist (iv) evaluating the entire cost of the empires (v) competition between imperialists (vi) revolution (vii) eradicating feeble empires and (viii) convergence. The mentioned stages are replicated until the convergence criterion is attained. At convergence point all empires collapse except the most powerful one. At this condition, all colonies have same positions and costs; competition ends and ICA stops. The flowchart summarizing the main steps of ICA is shown in Fig. 3 [46]. For additional aspect of ICA readers are advised to please refer [13,35,46]. The ICA input parameters are stated in Appendix [21].

3.3. Cost function

To fix the parameters of the controller, a cost function (J) is designed grounded on the anticipated provisions and restraints. Some of the classically used cost functions in engineering are the ISE (integral-squared error), ITSE (integral-time-multiplied-SE), IAE (integral-absolute error) and ITAE (integral-time-multiplied-AE) [21,37–39,42]. However, most adopted cost function is the ISE because it is easy to calculate and it permits to separate over-damped from underdamped system. The ISE squares the error to eradicate negative error components. It penalizes large errors more compared to smaller ones. It offers fast responses and allows small oscillations as the time goes. The result demonstrates that the ISE-based tuning has fewer number of iteration for global convergence compared to other methods. Hence, in this paper, because of decent recital of ISE, it is utilized as J [19,21,30,36–39,42]. The structure for ISE is given in Eq. (6) and other cost functions (J_S) are defined by Eqs. (7)–(9).

$$ISE = \int_0^T \left\{\Delta F_1^2 + \Delta F_2^2 + \Delta Ptie_{12}^2\right\} dt \tag{6}$$

$$ITSE = \int_0^T t\left\{\Delta F_1^2 + \Delta F_2^2 + \Delta Ptie_{12}^2\right\} dt \tag{7}$$

$$IAE = \int_0^T \{|\Delta F_1| + |\Delta F_2| + |\Delta Ptie_{12}|\} dt \tag{8}$$

$$ITAE = \int_0^T t\{|\Delta F_1| + |\Delta F_2| + |\Delta Ptie_{12}|\} dt \tag{9}$$

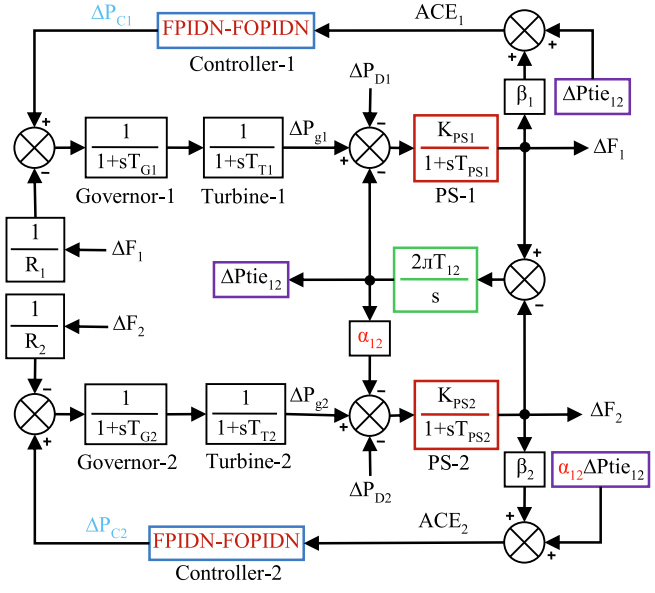

Fig. 4. Interconnected TANRT PS model [15].

Table 2
FPIDN/FPIDN-FOPIDN controller optimized parameters.

Parameters	TANRT PS		MSTATHG PS		TART PS	
	FPIDN	FPIDN-FOPIDN	FPIDN	FPIDN-FOPIDN	FPIDN	FPIDN-FOPIDN
K_P	2.9924	3.6547	2.4367	2.1651	1.5251	4.5240
K_I	4.9901	6.3651	3.8885	3.7542	2.9256	3.3647
K_D	1.5955	1.2456	0.3587	0.1365	0.1854	0.1621
N	490.2132	493.6358	266.3171	425.5684	401.8659	455.9645
K_{P1}	–	2.9247	–	3.0657	–	4.9546
K_{I1}	–	6.6854	–	2.8954	–	3.2561
λ	–	0.0885	–	0.5258	–	0.3521
K_{D1}	–	0.5994	–	0.2764	–	1.2912
μ	–	0.0164	–	0.2561	–	0.5784
N1	–	451.6845	–	488.3654	–	443.7628

where T is the simulation time range. ΔF_1, ΔF_2 and $\Delta Ptie_{12}$ are change in area-1 frequency, change in area-2 frequency and change in power of tie-line connecting areas 1 and 2, respectively. The J_S for three-area system can be defined consequently. The recital of the systems is obtained with the controller parameters acquired for lowest value of Eq. (6) via ICA. The values of the additional J_S in Eqs. (7)–(9) are calculated for comparison purpose. To be tuned parameters of the suggested FPIDN-FOPIDN controller are ten (K_P/K_I/K_D/N/K_{P1}/K_{I1}/λ/K_{D1}/μ/N1) and PIDN/FPIDN controller are four (K_P/K_I/K_D/N). The parameters of the controllers are optimized using ICA at slightest cost of (6) under the consideration of the constraints specified in (10).

$$\left.\begin{aligned} K_P^{min} \le K_P \le K_P^{max} \\ K_I^{min} \le K_I \le K_I^{max} \\ K_D^{min} \le K_D \le K_D^{max} \\ N^{min} \le N \le N^{max} \\ K_{P1}^{min} \le K_{P1} \le K_{P1}^{max} \\ K_{I1}^{min} \le K_{I1} \le K_{I1}^{max} \\ \lambda^{min} \le \lambda \le \lambda^{max} \\ K_{D1}^{min} \le K_{D1} \le K_{D1}^{max} \\ \mu^{min} \le \mu \le \mu^{max} \\ N1^{min} \le N1 \le N1^{max} \end{aligned}\right\} \quad (10)$$

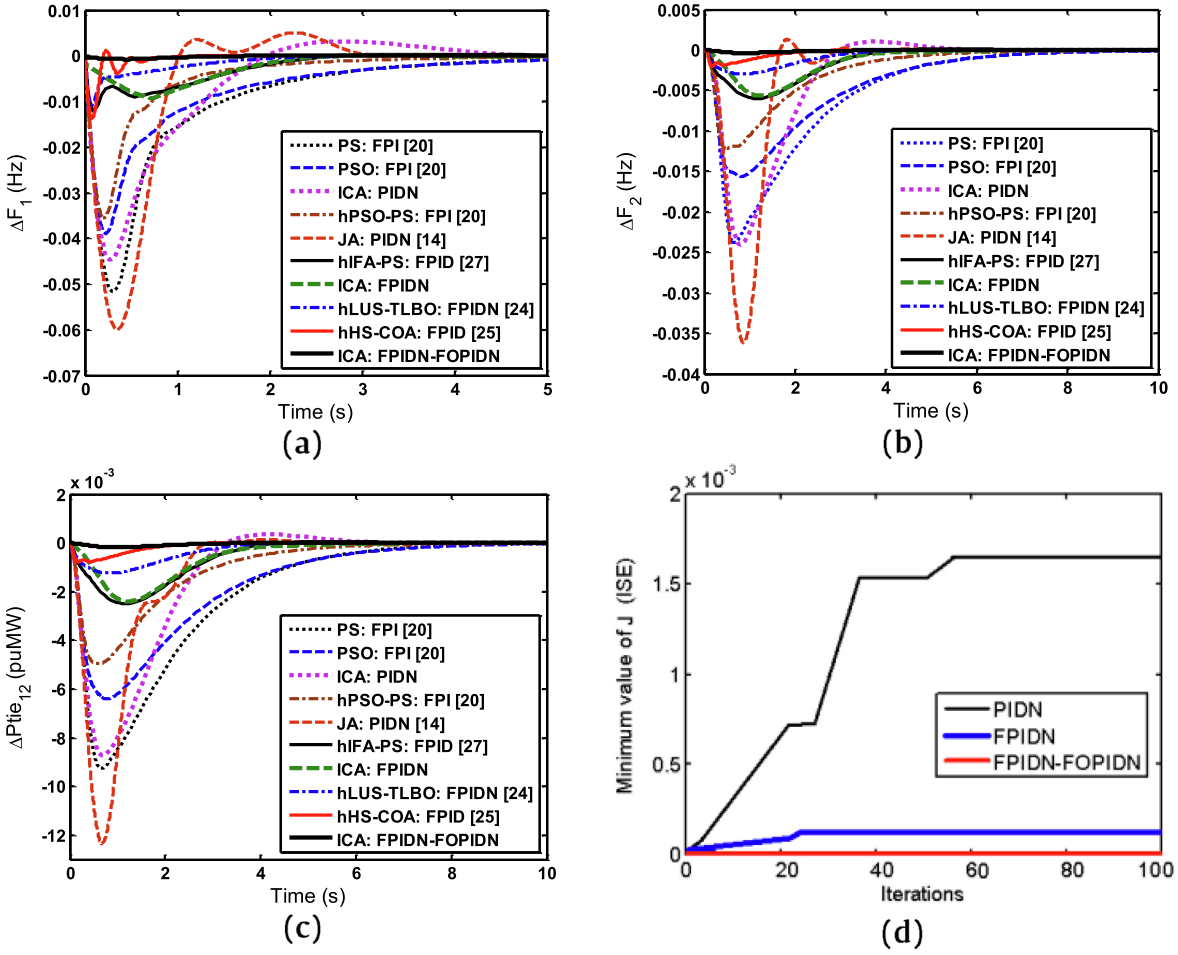

Fig. 5. TANRT PS responses under ΔP_{D1} = 0.05 puMW. (a) ΔF_1, (b) ΔF_2, (c) $\Delta Ptie_{12}$ and (d) evaluating the convergence appearances of ICA for PIDN/FPIDN/FPIDN-FOPIDN controller.

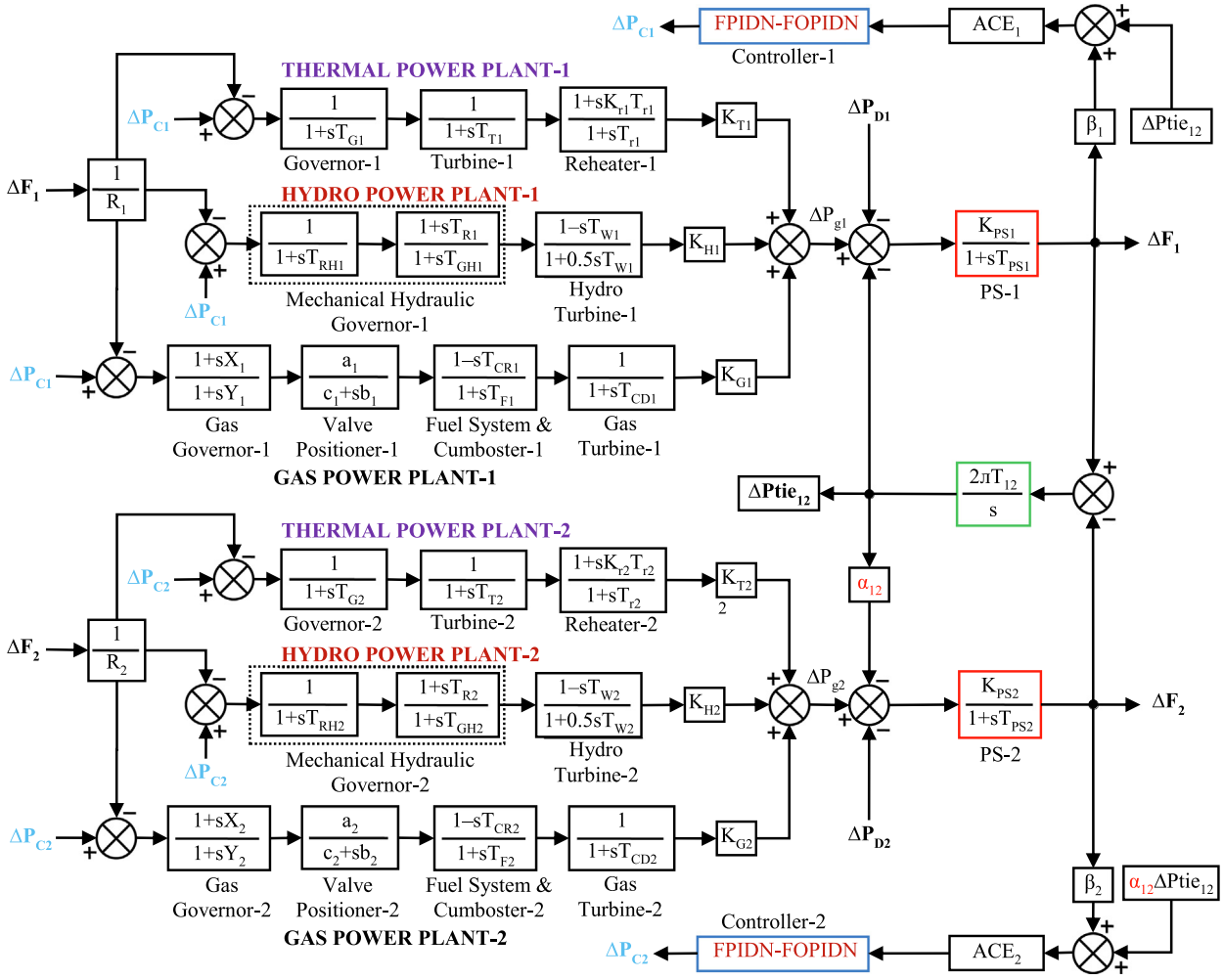

Fig. 6. TF model of MSTATHG PS [42].

Table 3
$T_S/U_S/O_S/J_S$ with TANRT PS at ΔP_{D1} = 0.05 puMW.

Controller structure	T_S (s)			U_S (−ve) (Hz)		U_S (−ve) (puMW)	O_S (Hz)		O_S (puMW)	J_S			
	ΔF_1	ΔF_2	$\Delta Ptie_{12}$	ΔF_1	ΔF_2	$\Delta Ptie_{12}$	ΔF_1	ΔF_2	$\Delta Ptie_{12}$	ISE	ITSE	IAE	ITAE
PS: FPI [20]	5.82	6.94	5.63	0.0516	0.0238	0.0092	0	0	0	$2.10e^{-3}$	$1.76e^{-3}$	0.1225	0.2054
PSO: FPI [20]	6.07	7.15	5.69	0.0389	0.0156	0.0064	0	0	0	$1.15e^{-3}$	$1.05e^{-3}$	0.0978	0.1827
ICA: PIDN	4.41	4.72	2.93	0.0446	0.0240	0.0087	$3.18e^{-3}$	$1.06e^{-3}$	$3.56e^{-4}$	$1.64e^{-3}$	$1.16e^{-3}$	0.0890	0.1044
hPSO-PS: FPI [20]	4.07	5.25	4.01	0.0355	0.0122	0.0059	0	0	0	$6.06e^{-4}$	$3.64e^{-4}$	0.0569	0.0799
JA: PIDN [14]	2.97	2.75	2.56	0.0600	0.0361	0.0123	$5.05e^{-3}$	$1.28e^{-3}$	$1.32e^{-4}$	$2.44e^{-3}$	$1.41e^{-3}$	0.0826	0.0686
hIFA-PS: FPID [27]	2.45	3.58	3.14	0.0120	0.0060	0.0025	$3.46e^{-4}$	$9.01e^{-5}$	$4.13e^{-5}$	$1.53e^{-4}$	$1.47e^{-4}$	0.0315	0.0430
ICA: FPIDN	2.38	2.74	2.55	0.0092	0.0056	0.0023	$5.83e^{-5}$	0	0	$1.22e^{-4}$	$1.36e^{-4}$	0.0280	0.0418
hLUS-TLBO: FPIDN [24]	2.05	3.06	2.36	0.0108	0.0029	0.0012	0	0	0	$4.19e^{-5}$	$2.79e^{-5}$	0.0148	0.0172
hHS-COA: FPID [25]	0.90	1.69	1.02	0.01400	0.00218	0.00080	$1.85e^{-3}$	0	0	$2.39e^{-5}$	$4.95e^{-6}$	0.0061	0.0042
ICA: FPIDN-FOPIDN	**0.84**	**0.89**	**1.00**	**0.00077**	**0.00038**	**0.00018**	0	0	0	$\mathbf{6.21e^{-7}}$	$\mathbf{5.12e^{-7}}$	**0.0020**	**0.0038**

Bold designates the best values.

Table 4
Comparative statistical analysis for different controllers.

Controllers	Minimum	Average	Worst	Standard deviation
PIDN	$1.64e^{-3}$	$1.93e^{-3}$	$3.17e^{-3}$	$0.42e^{-3}$
FPIDN	$1.22e^{-4}$	$1.55e^{-4}$	$2.71e^{-4}$	$0.28e^{-4}$
FPIDN-FOPIDN	$\mathbf{6.21e^{-7}}$	$\mathbf{9.07e^{-7}}$	$\mathbf{1.99e^{-6}}$	$\mathbf{0.81e^{-7}}$

Bold designates the best values.

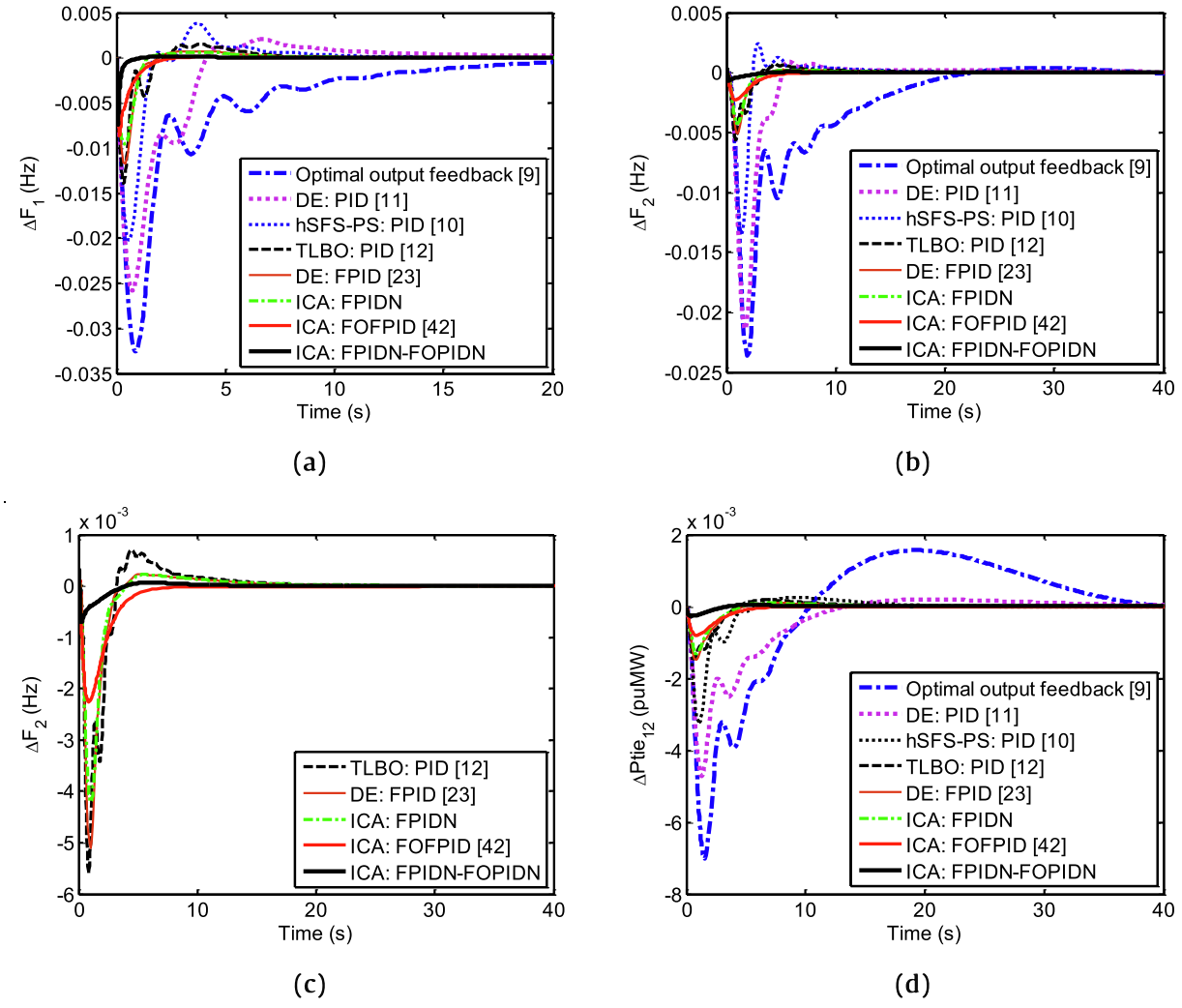

Fig. 7. Realistic MSTATHG PS responses under 1% SLP in area-1 at t = 0 s. (a) ΔF_1, (b) ΔF_2, (c) ΔF_2 with more clarity and (d) $\Delta Ptie_{12}$.

In (10), min and max represent the minimum and maximum parameter bounds of the controller. The optimization procedure is reiterated by 50 and the finest ultimate values of controller parameters obtained via ICA in 50 runs at minimum values of ISE are provided in Table 2 for the studied IPS models.

4. Simulation results

4.1. TANRT PS

The proposed controller is implemented upon a two-area non-reheat thermal (TANRT) PS. The system TF model is revealed in Fig. 4. The used nomenclature is provided in 'Description of symbols' and system data along with relevant references is specified in Appendix. The TANRT PS is simulated under a step load perturbation (SLP) of 5% puMW in area-1 (ΔP_{D1} = 0.05 puMW) at t = 0 s employing PIDN, FPIDN and FPIDN-FOPIDN controllers. The parameters of FPIDN and FPIDN-FOPIDN controllers obtained by means of ICA are provided in Table 2. However, tuned PIDN controller parameters are given in [37]. The PS dynamic responses of change in area-1 frequency (ΔF_1), change in area-2 frequency (ΔF_2) and change in power of tie-line ($\Delta Ptie_{12}$) are revealed in Fig. 5 (a-c). To manifest the dominance of cascade FPIDN-FOPIDN controller, its responses are equated with some existing control methods emerged recently in the literature such as PIDN controller tuned via jaya algorithm (JA) [14], fuzzy PI (FPI) controller tuned via PSO (particle swarm optimization)/PS (pattern search/hPSO-PS (hybrid PSO-PS) [20], FPID controller adjusted via hHS-COA (hybrid harmony search-cuckoo optimization algorithm) [25]/hIFA-PS (hybrid improved firefly algorithm-PS) [27], FPIDN controller tuned via hLUS-TLBO (hybrid local unimodal sampling-teaching learning based optimisation) [24] and ICA tuned PIDN/FPIDN controllers. It is evident from Fig. 5(a-c) that the offered cascade FPIDN-FOPIDN controller provides superior outcomes compared to other controllers regarding improved and fast oscillation free responses showing no over shoots and trivial peak under shoots. The superiority of the ICA optimized FPIDN-FOPIDN over ICA optimized FPIDN and ICA optimized PIDN controllers is also exposed from their convergence outcomes displayed in Fig. 5(d). Fig. 5(d) demonstrates that the cost function (J) i.e., ISE value corresponding to FPIDN-FOPIDN is smaller compared to FPIDN/PIDN. Moreover, FPIDN-FOPIDN controller converges faster compared to FPIDN/PIDN controller.

To scrutinize the recital of the recommended controller measurably, the numeric quantities of different J_S discussed in Eqs. (6)–(9) are computed. The J_S values support in constructing a perceptible relative examination about the concert of the suggested controller with the techniques prevailing in the literature. Therefore, settling

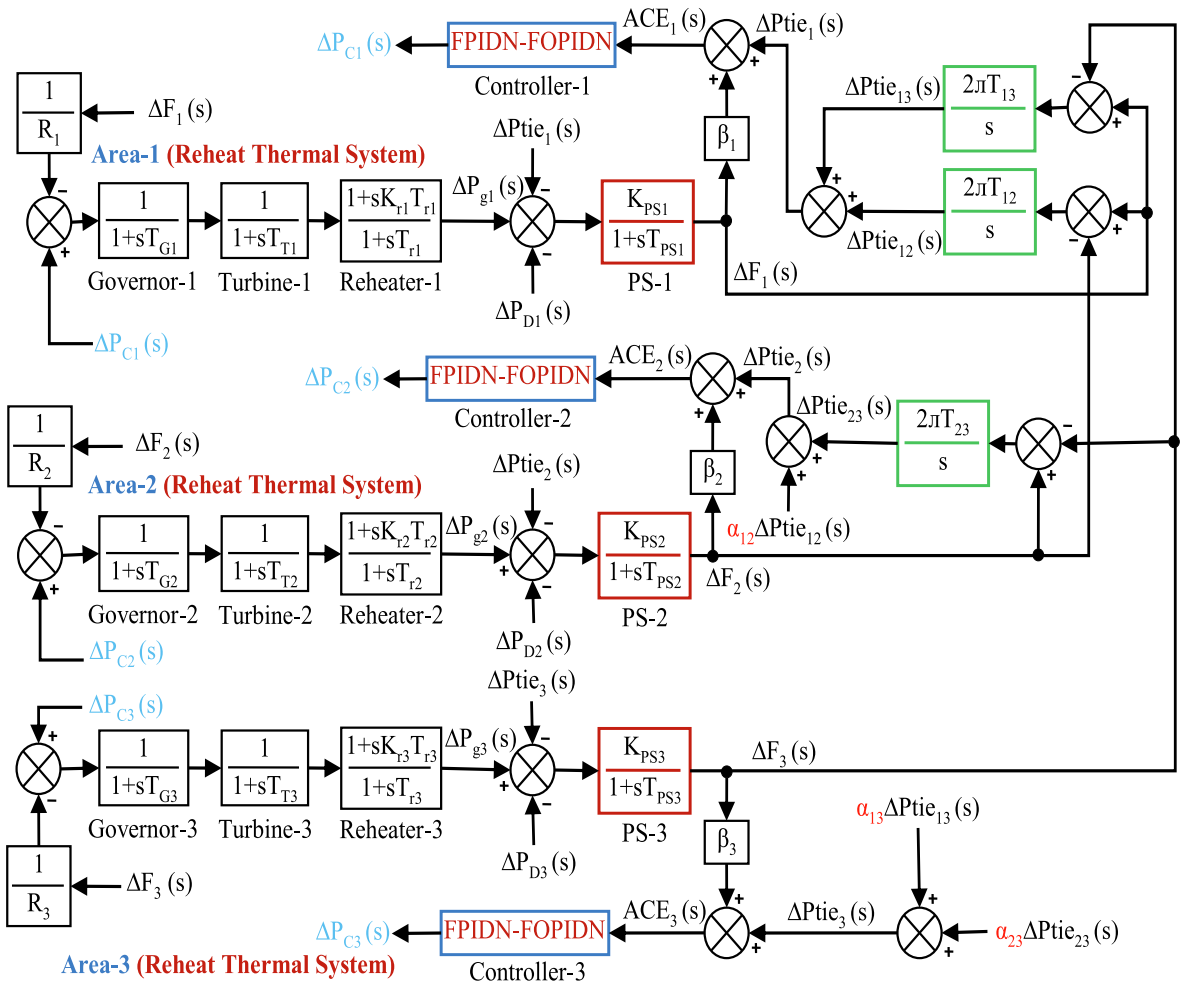

Fig. 8. TF model of TART PS [8].

Table 5
$T_S/U_S/O_S/J_S$ with MSTATHG PS at ΔP_{D1} = 0.01 puMW.

Controller structure	T_S (s)			U_S (−ve) (Hz)		U_S (−ve) (puMW)	J_S			
	ΔF_1	ΔF_2	$\Delta Ptie_{12}$	ΔF_1	ΔF_2	$\Delta Ptie_{12}$	ISE	ITSE	IAE	ITAE
Optimal output feedback [9]	19.87	19.55	31.98	0.03250	0.02360	0.00700	$2.59e^{-3}$	$6.60e^{-3}$	0.2255	1.0460
DE: PID [11]	13.09	8.52	9.22	0.02580	0.02150	0.00471	$1.39e^{-3}$	$2.14e^{-3}$	0.1201	0.3467
hSFS-PS: PID [10]	8.58	7.34	3.88	0.02020	0.01340	0.00325	$4.84e^{-4}$	$5.31e^{-4}$	0.0587	0.1600
TLBO: PID [12]	6.27	5.805	2.79	0.01390	0.00559	0.00146	$1.11e^{-5}$	$9.62e^{-5}$	0.0286	0.0773
DE: FPID [23]	5.12	2.69	2.53	0.01180	0.00509	0.00149	$9.56e^{-5}$	$6.68e^{-5}$	0.0229	0.0530
ICA: FPIDN	4.99	2.53	2.25	0.00955	0.00420	0.00131	$7.29e^{-5}$	$5.18e^{-5}$	0.0206	0.0498
ICA: FOFPID [42]	1.79	3.34	2.22	0.00865	0.00226	0.00080	$3.33e^{-5}$	$2.09e^{-5}$	0.0133	0.0225
ICA: FPIDN-FOPIDN	**0.51**	**0.63**	**0.59**	**0.00734**	**0.00071**	**0.00026**	$\mathbf{5.90e^{-6}}$	$\mathbf{1.38e^{-6}}$	**0.0041**	**0.0091**

Bold designates the best values.

time (T_S), maximum under shoot (U_S), maximum over shoot (O_S) of $\Delta F_1/\Delta F_2/\Delta Ptie_{12}$ results and J_S (ISE/ITSE/IAE/ITAE) are calculated while conducting MATLAB simulation and shown in Table 3. From this table, it is observed that the mathematical outputs of T_S, U_S, O_S and ISE/ITSE/IAE/ITAE by FPIDN-FOPIDN controller are observed least than other methods. Consequently, it is clearly identified from Fig. 5(a-c) and Table 3 that the results of FPIDN-FOPIDN controller are smooth with lowest $U_S/O_S/J_S$ and correctly reach to the preferred zero steady state values in minimum time under a SLP in a control area compared to JA [14]/ICA: PIDN, PSO/PS/hPSO-PS: FPI [20], hHS-COA [25]/hIFA-PS [27]: FPID and ICA/hLUS-TLBO [24]: FPIDN controllers. Hence, the offered controller demonstrates better dynamic performance in AGC of PS industry. It is to be recognized that T_S of the output results is considered for an error band of ±0.0005 [21,30,37–39,42] around the final value and J_S is computed for a SIMULINK run time of 15 s [21] regarding each IPS models under the study.

To guarantee the solidity of the recommended controller, a statistical investigation is also conducted. The ICA tuning procedure was continual for 50 times for each controller and standard deviation (SD), minimum, average and worst of ISE values computed with FPIDN and FPIDN-FOPIDN controllers are collected for the statistical study in Table 4. It is plainly stripped from Table 4 that the FPIDN-FOPIDN controller displays the lowest values of SD,

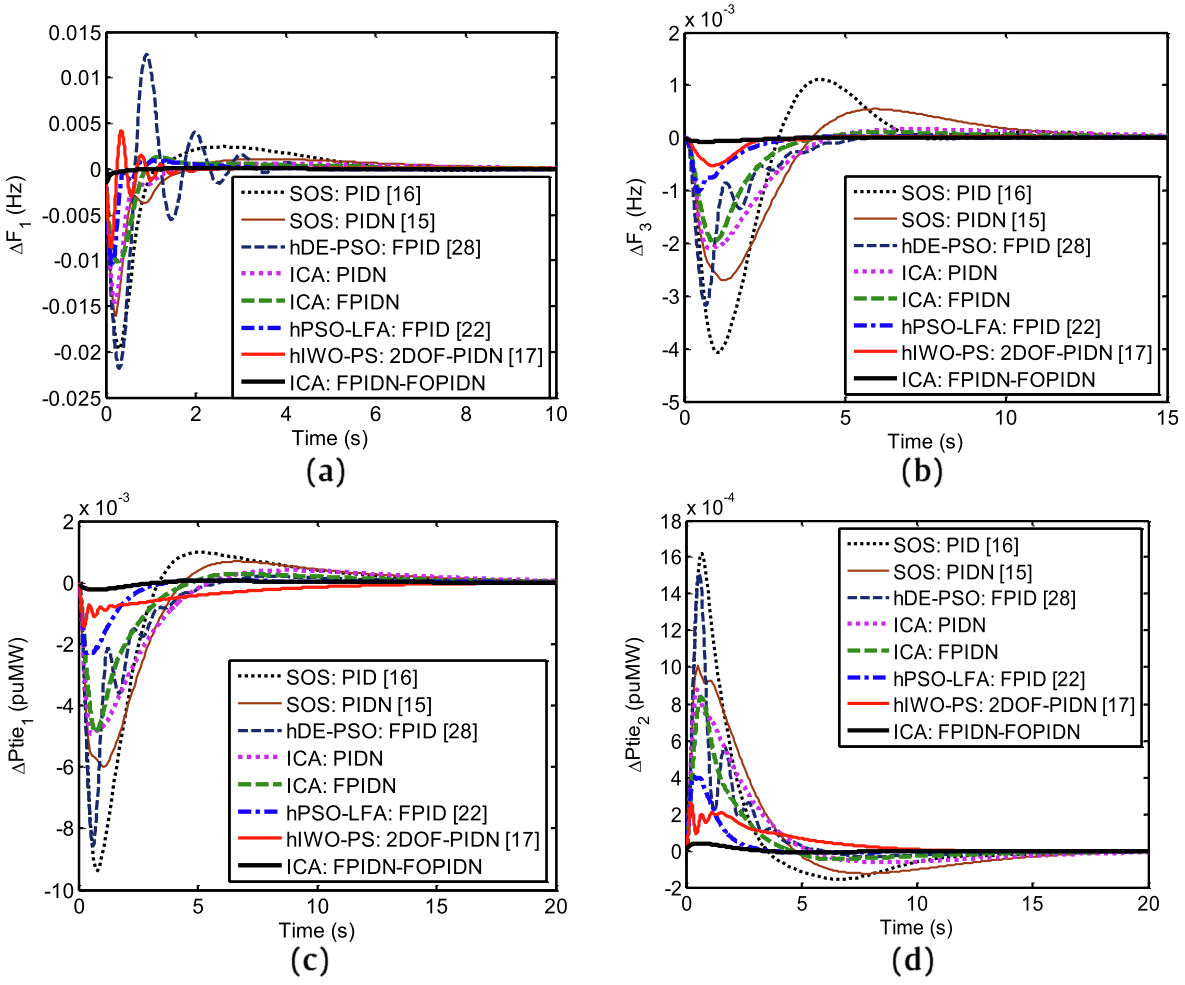

Fig. 9. TART PS responses under 2% SLP in area-1 at t = 0 s. (a) ΔF_1, (b) ΔF_3, (c) $\Delta Ptie_1$ and (d) $\Delta Ptie_2$.

Table 6
$T_S/U_S/O_S/J_S$ with TART PS at ΔP_{D1} = 0.02 puMW.

Controller structure	T_S (s)			U_S (−ve) (Hz)			O_S (Hz)		O_S (puMW)	J_S			
	ΔF_1	ΔF_2	ΔF_3	ΔF_1	ΔF_2	ΔF_3	ΔF_1	ΔF_2	ΔF_3	ISE	ITSE	IAE	ITAE
SOS: PID [16]	5.54	5.63	5.78	0.0196	0.0048	0.0040	0.0024	0.0011	0.0011	$2.64e^{-4}$	$2.33e^{-4}$	0.0592	0.1495
SOS: PIDN [15]	6.65	6.43	6.84	0.0160	0.0030	0.0027	$1.09e^{-3}$	$5.20e^{-4}$	$5.48e^{-4}$	$1.38e^{-4}$	$1.37e^{-4}$	0.0488	0.1499
ICA: PIDN	4.94	2.98	3.14	0.0146	0.0026	0.0020	0.0006	0.0001	0.0001	$9.30e^{-5}$	$7.20e^{-5}$	0.0356	0.1050
hDE-PSO: FPID [28]	4.20	2.92	2.98	0.0218	0.0040	0.0031	0.0126	0	0	$2.50e^{-4}$	$1.51e^{-4}$	0.0406	0.0701
ICA: FPIDN	3.37	2.20	2.37	0.0101	0.002289	0.001968	$1.29e^{-3}$	$1.28e^{-4}$	0	$6.54e^{-5}$	$4.28e^{-5}$	0.0261	0.0607
hPSO-LFA: FPID [22]	1.97	1.24	1.27	0.0105	0.001083	0.001023	$9.45e^{-4}$	0	0	$2.34e^{-5}$	$7.58e^{-6}$	0.0105	0.0151
hIWO-PS: 2DOF-PIDN [17]	1.50	1.01	1.09	0.0085	0.00070	0.00052	$4.19e^{-3}$	0	0	$1.44e^{-5}$	$7.58e^{-6}$	0.0109	0.0360
ICA: FPIDN-FOPIDN	**0.15**	**0.51**	**0.58**	**0.0014**	**0.000085**	**0.000071**	**$6.77e^{-5}$**	0	0	**$2.45e^{-7}$**	**$1.65e^{-7}$**	**0.0017**	**0.0058**

Bold designates the best values.

minimum, average and worst. Table 4 indicates that minimum ISE is obtained with the FPIDN-FOPIDN (ISE = $6.21e^{-7}$) compared to FPIDN (ISE = $1.22e^{-4}$) and PIDN (ISE = $1.64e^{-3}$) controllers tuned via ICA. Table 4 also states that, FPIDN-FOPIDN controller displays superior performance over FPID/FPIDN concerning slightest values for SD, minimum, average and worst. Hence, the statistical study concludes that the suggested controller is better in comparison to PIDN/FPIDN controller for AGC problem solution in TANRT PS.

4.2. Realistic MSTATHG PS

To authorize the preeminence and practicability of the recommended control approach, the methodology is next protracted to a more realistic multi-source two-area thermal-hydro-gas (MSTATHG) PS prevailing in the recent literature [9–12,23,42]. The TF model of the PS is exhibited in Fig. 6. Every area of PS comprises of realistic multi-source power plants like reheat thermal, mechanical governor based hydro and gas generating plants. The parameters of the PS are given in Appendix.

The system model is simulated at 1% SLP at t = 0 s in area-1. ICA adjusted parameters of FPIDN and cascade FPIDN-FOPIDN controllers are given in Table 2. The system dynamic responses for ΔF_1, ΔF_2 and $\Delta Ptie_{12}$ are revealed in Fig. 7. The recital of the suggested ICA boosted cascade FPIDN-FOPIDN controller is contrasted with ICA optimized FPIDN controller, optimal output feedback controller [9] and various recent controllers like hSFS-PS [10]/DE

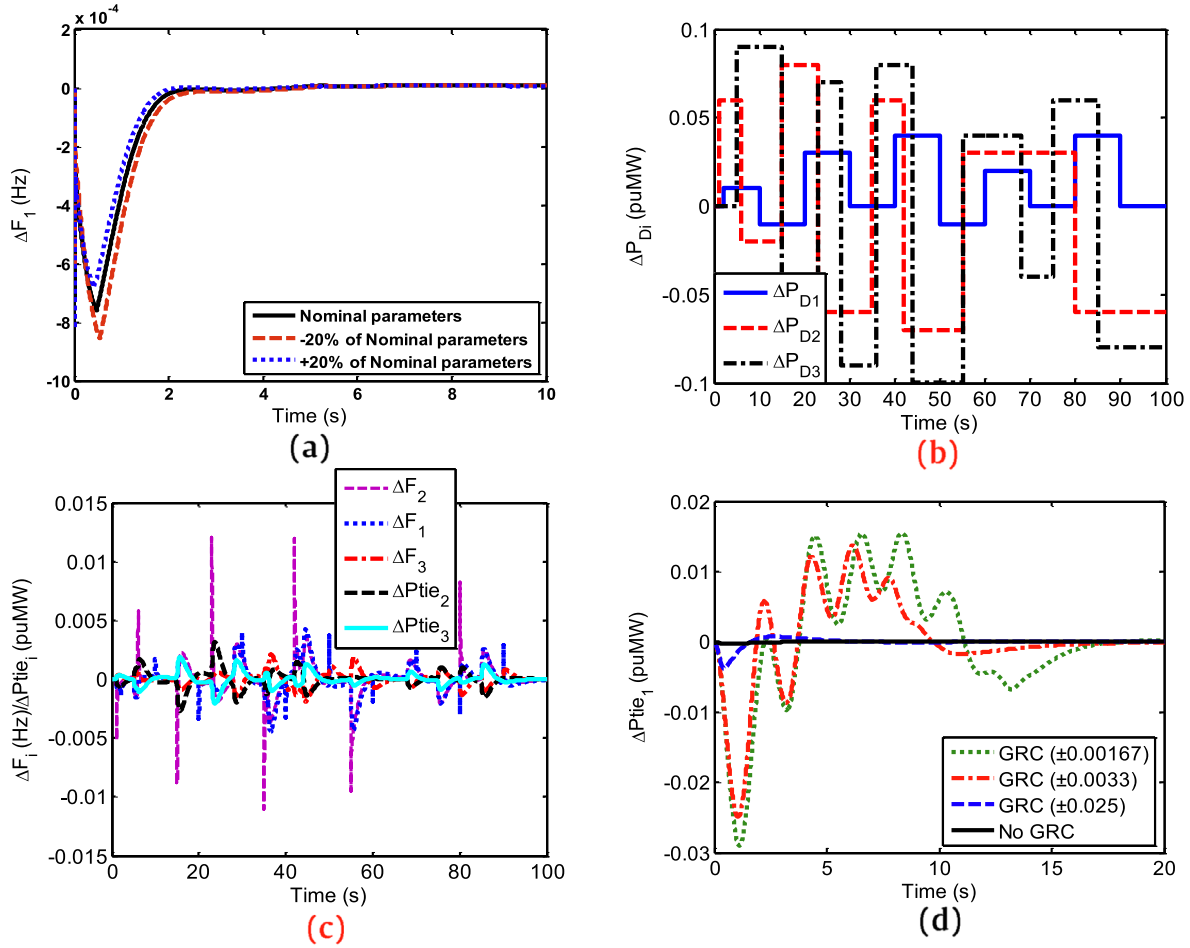

Fig. 10. Responses of PSs under robustness investigation. (a) ΔF_1 of TANRT system under changed parameters, (b) simultaneous variable SLPs in all areas of TART, (c) $\Delta F_1/\Delta F_2/\Delta F_3/\Delta Ptie_2/\Delta Ptie_3$ of TART system under variable SLPs in all areas and (d) $\Delta Ptie_1$ of TART system with/without GRC under 2% SLP in area-1.

[11]/TLBO [12] adjusted PID, DE [23] optimized FPID and ICA [42] optimized FOFPID controllers as revealed in Fig. 7 and Table 5. It is revealed from Fig. 7/Table 5 that the FPIDN-FOPIDN controller outperforms all other controllers in terms of lowest T_S (ΔF_1 = 0.51 s, ΔF_2 = 0.63 s and $\Delta Ptie_{12}$ = 0.59 s), U_S (ΔF_1 = −0.00734 Hz, ΔF_2 = −0.00071 Hz and $\Delta Ptie_{12}$ = −0.00026 puMW) and J_S (ISE = 5.90e^{-6}, ITSE = 1.38e^{-6}, IAE = 0.0041 and ITAE = 0.0091) values for ΔF_1, ΔF_2 and $\Delta Ptie_{12}$ responses. Therefore, the suggested approach can be implemented successfully to realistic multi-area multi-source system and delivers superior transient and steady state results in comparison to numerous approaches widespread in the latest literature.

4.3. TART PS

To convey the skill and scalability of the method in multi-area system, furthermore, the study is prolonged to an unequal three-area reheat thermal (TART) PS presented in Fig. 8 [8]. The ratings of area-1, area-2 and area-3 are 2000 MW, 5000 MW and 8000 MW, in order. Consequently, area size ratios $\alpha_{12}/\alpha_{13}/\alpha_{23}$ are −2/5/−2/8/−5/8, respectively. The responses of the system under a SLP of 2% in area-1 at t = 0 s with ICA based PIDN/FPIDN/FPIDN-FOPIDN controller and just published SOS optimized PID [16], SOS optimized PIDN [15], hPSO-LFA [22]/hDE-PSO [28] optimized FPID and hIWO-PS optimized 2DOF-PIDN [17] controllers are shown in Fig. 9(a-d) for change in area frequency signals i.e., ΔF_1, ΔF_2 and change in area tie-line flow signals i.e., $\Delta Ptie_1$ and $\Delta Ptie_2$. The system results in terms of $O_S/U_S/T_S/J_S$ are depicted in Table 6. It is revealed from the inspection of Fig. 9(a-d) and Table 6 that the suggested approach performs superbly and shows admirable performance in comparison to other existing and designed controllers for an interconnected TART AGC system. Hence, the recommended controller fulfills the desired requirement of a suitable secondary controller for AGC problem solution of interconnected electric PSs.

5. Robustness study

A robustness analysis is conducted to check the performance and sturdiness of the suggested ICA optimized FPIDN-FOIPIDN controller at wide variations in the system operating conditions. To illustrate the robustness of the suggested control strategy, the PS model parameters are altered ±20% from the values provided in Appendix. The considered controller must behave toughly devoid of ample deterioration in the PS performance at parameter deviations. Fig. 10(a) shows ΔF_1 result of TANRT at nominal and ±20% changed parameters. The assessment of Fig. 10(a) clearly divulges that all the responses are more or less same and they do not deviate much from the nominal response.

To illustrate the superiority as well as robustness of the proposed control method designed at SLP in area-1, random load patterns of different duration and extent are used simultaneously in all control

areas of TART system as shown in Fig. 10(b). From ΔF_1, ΔF_2, ΔF_3, $\Delta Ptie_2$ and $\Delta Ptie_3$ dynamic responses of TART system shown in Fig. 10(c), it can be observed that the FPIDN-FOPIDN controller attains the best stabilized performance following random load variations. It should be noted that the system will become unstable under random load changes if the designed controller is not robust.

Further, in PS, the generation of power can vary only at a specific extreme rate because of the restrictions of thermal and mechanical actions termed as generation rate constraint (GRC). If GRC is not included, system is expected to follow large brief usual disturbances occurring in PS and which is not desired. Thus, GRC essentially be incorporated in PS for a realistic AGC study. The TART system is simulated via the proposed method without and with the considering closed loop GRC limits of ±0.025 pu/s, 0.0033 pu/s and 0.00167 pu/s in thermal turbines as shown in Fig. 10(d) for $\Delta Ptie_1$. From Fig. 10(d), it is perceived that the occurrence of GRC results in larger oscillations/U_S/O_S/T_S with the proposed controller optimized for the linear system. However, the dynamic responses of the PS with GRC gratifies AGC problem obligation without loss of system stability, which signifies the robustness of the controller. It is witnessed if we dwindle GRC value for reheat thermal unit, the dynamic results of the PS depreciate appreciably.

In overall, Fig. 10(a-d) indicate that all the responses due to the proposed controller optimized for the linear systems (with the gains shown in Table 2) are stable under wide variations in the parameters, random load demands and GRC values. Consequently, the presented controller conducts robustly under varied operating environments and its gains adjusted at nominal conditions are not needed to be re-tuned.

6. Conclusion

A novel ICA optimized cascaded FPIDN-FOPIDN controller is suggested for AGC of multi-area PSs. Initially, a TANRT PS is scrutinized in the presence of 5% SLP in area-1. The PS results due to the suggested controller are equated with JA optimized PIDN, hPSO-PS/PSO/PS optimized FPI, hIFA-PS/hHS-COA tuned FPID, hLUS-TLBO tuned FPIDN controllers stated in the latest literature and ICA optimized PIDN/FPIDN controllers. It is noted that significant development in terms of oscillation free results with minimum quantities of T_S/U_S/O_S/J_S are acquired with the ICA optimized FPIDN-FOPIDN controller over other controllers. To further validate the capability, extensibility and advantage of the method for other systems, the study is extended to realistic MSTATHG and TART PSs. The asset of ICA tuned FPIDN-FOPIDN controller is established over optimal output feedback, intelligent DE/hSFS-PS/SOS/TLBO optimized PID, SOS/ICA tuned PIDN, DE/hDE-PSO/hPSO-LFA tuned FPID, ICA tuned FPIDN/FOFPID and hIWO-PS tuned 2DOF-PIDN controllers. Lastly, a robustness investigation is conducted to express the performance and strength of the proposed controller under ±20% deviations in all the parameters of the PSs, random power load demands in multiple areas and appropriate GRC. It is detected that the proposed controller designed at nominal condition is robust and shows stable performance with wide deviations in the system parameters, load patterns and GRC values. Furthermore, with higher GRC, superior responses with smaller peak deviation and lesser settling time are observed. In future, the work may be extended to modern interconnected restructured PSs utilizing more recent optimization techniques.

Declaration of Competing Interest

The authors declare that they have no known competing financial interests or personal relationships that could have appeared to influence the work reported in this paper.

Appendix

Parameters of ICA: [21]:

No of countries = 500, No of iterations = 100, Assimilation angle coefficient (γ) = 0.5, No of initial empires = 40; No of initial colonies = 500–40 = 460; Assimilation coefficient (β) = 1.5, Coefficient associated with average power of empire's colonies (ξ) = 0.05, Revolution rate (pr) = 0.3.

PSs data:

TANRT PS [20]:

P_{ri} = 2000 MW, $\alpha_{12} = -1$, T_{PSi} = 20 s, K_{PSi} = 120 Hz/puMW, T_{Ti} = 0.3 s, T_{Gi} = 0.03 s, R_i = 2.4 Hz/puMW, $2\pi T_{12}$ = 0.545 puMW/Hz, β_i = 0.425 puMW/Hz, F^0 = 60 Hz, initial loading = 50%.

Realistic MSTATHG PS [42]:

P_{ri} = 2000 MW, T_{PS} = 11.49 s, K_{PS} = 68.9655 Hz/puMW, $\alpha_{12} = -1$, β = 0.4312 puMW/Hz, R = 2.4 Hz/puMW, T_T = 0.3 s, T_G = 0.06 s, T_r = 10.2 s, K_r = 0.3, T_R = 4.9 s, T_{RH} = 28.749 s, T_W = 1.1 s, T_{GH} = 0.2 s, Y = 1.1 s, X = 0.6 s, b = 0.049 s, a = c = 1, T_F = 0.239 s, T_{CR} = 0.01 s, T_{CD} = 0.2 s; K_T = 0.5747; K_H = 0.2873; K_G = 0.1380, T_{12} = 0.0433, initial loading = 1740 MW, F^0 = 60 Hz,

TART PS [8]:

P_r = 2000 MW, P_n = 50%, F^0 = 60 Hz, β_i = 0.425 puMW/Hz, R_i = 2.4 Hz/puMW, T_{Gi} = 0.08 s, T_{Ti} = 0.3 s, K_{ri} = 0.5, T_{ri} = 10 s, K_{PSi} = 120, T_{PSi} = 20 s, T_{12} = 0.0866 puMW/rad, $\alpha_{12} = -2/5$, $\alpha_{13} = -2/8$, $\alpha_{23} = -5/8$.

References

[1] K.S. Simhadri, B. Mohanty, S.K. Panda, Comparative performance analysis of 2DOF state feedback controller for automatic generation control using whale optimization algorithm, Optim. Contr. Appl. Methods 40 (1) (2019) 24–42.
[2] A. Pappachen, A.P. Fathima, Critical research areas on load frequency control issues in a deregulated power system: A state-of-the-art-of-review, Renewab. Sustainb. Energy Rev. 72 (2017) 163–177.
[3] A. Latif, S.M.S. Hussain, D.C. Das, T.S. Ustun, State-of-the-art of controllers and soft computing techniques for regulated load frequency management of single/multi-area traditional and renewable energy based power systems, Appl. Energy 266 (2020) 114858.
[4] X. Liu, Y. Zhang, K.Y. Lee, Coordinated distributed MPC for load frequency control of power system with wind farms, IEEE Trans. Ind. Electron. 64 (6) (2017) 5140–5150.
[5] X. Liu, Y. Zhang, K.Y. Lee, Robust distributed MPC for load frequency control of uncertain power systems, Contr. Eng. Practice. 56 (6) (2016) 136–147.
[6] X. Liu, X. Kong, K.Y. Lee, Distributed MPC for load frequency control with dynamic fuzzy valve position modeling for hydro-thermal power system, IET Contr. Theory Appl. 10 (14) (2016) 1653–1664.
[7] Y. Arya, N. Kumar, S.K. Gupta, Optimal automatic generation control of two-area power systems with energy storage units under deregulated environment, J. Renewab. Sustainab. Energy. 9 (6) (2017) 064105–64120.
[8] P. Dahiya, P. Mukhija, A.R. Saxena, Y. Arya, Comparative performance investigation of optimal controller for AGC of electric power generating systems, Automatika: J. Contr. Meas.r Electron. Comput. Communicat. 57 (4) (2016) 902–921.
[9] K.P.S. Parmar, S. Majhi, D.P. Kothari, Improvement of dynamic performance of LFC of the two area power system: an analysis using MATLAB, Int. J. Comput. Appl. 40 (10) (2012) 28–32.
[10] S. Padhy, S. Panda, A hybrid stochastic fractal search and pattern search technique based cascade PI-PD controller for automatic generation control of multi-source power systems in presence of plug in electric vehicles, CAAI Trans. Intel. Tech. 2 (1) (2017) 12–25.
[11] B. Mohanty, S. Panda, P.K. Hota, Controller parameters tuning of differential evolution algorithm and its application to load frequency control of multi-source power system, Int. J. Elect. Power Energy Syst. 54 (2014) 77–85.
[12] A.K. Barisal, Comparative performance analysis of teaching learning based optimization for automatic load frequency control of multi-source power systems, Int. J. Elect. Power Energy Syst. 66 (2015) 67–77.
[13] H. Shabani, B. Vahidi, M. Ebrahimpour, A robust PID controller based on imperialist competitive algorithm for load-frequency control of power systems, ISA Trans. 52 (1) (2013) 88–95.
[14] S.P. Singh, T. Prakash, V.P. Singh, M.G. Babu, Analytic hierarchy process based automatic generation control of multi-area interconnected power system using jaya algorithm, Eng. Appl. Artificial Intel. 60 (2) (2017) 35–44.
[15] H.M. Hasanien, A. El-Fergany, Symbiotic organisms search algorithm for automatic generation control of interconnected power systems including wind farms, IET Gener. Transm. Distrib. 11 (7) (2017) 1692–1700.

[16] D. Guha, P.K. Roy, S. Banerjee, Symbiotic organism search algorithm applied to load frequency control of multi-area power system, Energy Syst. 9 (2) (2018) 439–468.
[17] N. Manoharan, S.S. Dash, K.S. Rajesh, S. Panda, Automatic generation control by hybrid invasive weed optimization and pattern search tuned 2-DOF PID controller, Int. J. Comput. Communicat. Contr. 12 (4) (2017) 533–549.
[18] W. Tasnin, L.C. Saikia, M. Raju, Deregulated AGC of multi-area system incorporating dish-Stirling solar thermal and geothermal power plants using fractional order cascade controller, Int. J. Elect. Power Energy Syst. 101 (2018) 60–74.
[19] A. Saha, L.C. Saikia, Load frequency control of a wind-thermal-split shaft gas turbine-based restructured power system integrating FACTS and energy storage devices, Int. Trans. Elect. Energy Syst. 29 (3) (2019) e2756.
[20] R.K. Sahu, S. Panda, G.T.C. Sekhar, A novel hybrid PSO-PS optimized fuzzy PI controller for AGC in multi area interconnected power systems, Int. J. Elect. Power Energy Syst. 64 (2015) 880–893.
[21] Y. Arya, Automatic generation control of two-area electrical power systems via optimal fuzzy classical controller, J. Franklin Inst. 355 (5) (2018) 2662–2688.
[22] A.K. Barisal, T.K. Panigrahi, S. Mishra, A hybrid PSO-levy flight algorithm based fuzzy PID controller for automatic generation control of multi area power systems: fuzzy based hybrid PSO for automatic generation control, Int. J. Energy Optimizat. Eng. 6 (2) (2017) 42–63.
[23] B.K. Sahu, T.K. Pati, J.R. Nayak, S. Panda, S.K. Kar, A novel hybrid LUS-TLBO optimized fuzzy-PID controller for load frequency control of multi-source power system, Int. J. Elect Power Energy Syst. 74 (2016) 58–69.
[24] P.K. Mohanty, B.K. Sahu, T.K. Pati, S. Panda, S.K. Kar, Design and analysis of fuzzy PID controller with derivative filter for AGC in multi-area interconnected power system, IET Gener. Transm. Distrib. 10 (15) (2016) 3764–3776.
[25] M. Gheisarnejad, An effective hybrid harmony search and cuckoo optimization algorithm based fuzzy PID controller for load frequency control, Appl. Soft Comput. 65 (2018) 121–138.
[26] A. Fathy, A.M. Kassem, A.Y. Abdelaziz, Optimal design of fuzzy PID controller for deregulated LFC of multi-area power system via mine blast algorithm, Neural Comput. Appl. 32 (9) (2020) 4531–4551, https://doi.org/10.1007/s00521-018-3720-x.
[27] K.S. Rajesh, S.S. Dash, R. Rajagopal, Hybrid improved firefly-pattern search optimized fuzzy aided PID controller for automatic generation control of power systems with multi-type generations, Swarm Evol. Comput. 44 (2019) 200–211.
[28] B.K. Sahu, S. Pati, S. Panda, Hybrid differential evolution particle swarm optimisation optimised fuzzy proportional-integral derivative controller for automatic generation control of interconnected power system, IET Gener. Transm. Distrib. 8 (11) (2014) 1789–1800.
[29] S. Dadfar, K. Wakil, M. Khaksar, A. Rezvani, M.R. Miveh, M. Gandomkar, Enhanced control strategies for a hybrid battery/photovoltaic system using FGS-PID in grid-connected mode, Int. J. Hydrogen Energy 44 (29) (2019) 14642–14660.
[30] Y. Arya, AGC of two-area electric power systems using optimized fuzzy PID with filter plus double integral controller, J. Franklin Inst. 355 (11) (2018) 4583–4617.
[31] A. Rezvani, A. Esmaeily, H. Etaati, M. Mohammadinodoushan, Intelligent hybrid power generation system using new hybrid fuzzy-neural for photovoltaic system and RBFNSM for wind turbine in the grid connected mode, Front Energy. 13 (1) (2019) 131–148.
[32] A. Rezvani, M. Gandomkar, Modeling and control of grid connected intelligent hybrid photovoltaic system using new hybrid fuzzy-neural method, Sol. Energy 127 (2016) 1–18.
[33] A. Rezvani, M. Gandomkar, Simulation and control of intelligent photovoltaic system using new hybrid fuzzy-neural method, Neural Comput. Appl. 28 (9) (2017) 2501–2518.
[34] N. Kumar, B. Tyagi, V. Kumar, Application of fractional order PID controller for AGC under deregulated environment, Int. J. Automat. Comput. 15 (1) (2018) 84–93.
[35] S.A. Taher, M.H. Fini, S.F. Aliabadi, Fractional order PID controller design for LFC in electric power systems using imperialist competitive algorithm, Ain Shams Eng. J. 5 (1) (2014) 121–135.
[36] A. Prakash, S. Murali, R. Shankar, R. Bhushan, HVDC tie-link modeling for restructured AGC using a novel fractional order cascade controller, Elect Power Syst Res. 170 (2019) 244–258.
[37] Y. Arya, Improvement in automatic generation control of two-area electric power systems via a new fuzzy aided optimal PIDN-FOI controller, ISA Trans. 80 (2018) 475–490.
[38] Y. Arya, Impact of ultra-capacitor on automatic generation control of electric energy systems using an optimal FFOID controller, Int. J. Energy Res. 43 (14) (2019) 8765–8778.
[39] Y. Arya, A new optimized fuzzy FOPI-FOPD controller for automatic generation control of electric power systems, J. Franklin Inst. 356 (11) (2019) 5611–5629.
[40] N.C. Patel, B.K. Sahu, D.P. Bagarty, P. Das, M.K. Debnath, A novel application of ALO-based fractional order fuzzy PID controller for AGC of power system with diverse sources of generation, Int. J. Elect. Eng. Educat. (2019), https://doi.org/10.1177/0020720919829710.
[41] R. Mohammadikia, M. Aliasghary, A fractional order fuzzy PID for load frequency control of four-area interconnected power system using biogeography-based optimization, Int. Trans. Elect. Energy Syst. 29 (2) (2019) e2735.
[42] Y. Arya, AGC performance enrichment of multi-source hydrothermal gas power systems using new optimized FOFPID controller and redox flow batteries, Energy. 127 (2017) 704–715.
[43] Z. Shao, K. Wakil, M. Usak, M.A. Heidari, B. Wang, R. Simoes, Kriging empirical mode decomposition via support vector machine learning technique for autonomous operation diagnosing of CHP in microgrid, Appl. Thermal Eng. 145 (2018) 58–70.
[44] X. Shi, A. Dini, Z. Shao, N.H. Jabarullah, Z. Liu, Impacts of photovoltaic/wind turbine/microgrid turbine and energy storage system for bidding model in power system, J. Cleaner Prod. 226 (2019) 845–857.
[45] D. Deepika, S. Kaur, S. Narayan, Centralized sliding mode frequency regulation approach for an uncertain islanded micro grid integrated with disturbance observer, Asian J. Contr. 21 (4) (2019) 2038–2048.
[46] E. Atashpaz-Gargari, C. Lucas, Imperialist competitive algorithm: an algorithm for optimization inspires by imperialistic competition, in: IEEE Congress on Evolutionary Computation, Singapore, Sep. 25-28, 2007, pp. 4661–4667.